

Studies on the Mechanism of Hypoxic Selectivity in Copper Bis(Thiosemicarbazone) Radiopharmaceuticals

Richard I. Maurer,[†] Philip J. Blower,^{*,‡} Jonathan R. Dilworth,^{*,§} Christopher A. Reynolds,^{*,†} Yifan Zheng,^{†,§} and Gregory E. D. Mullen[§]

Department of Biological Sciences, University of Essex, Wivenhoe Park, Colchester CO4 3SQ, United Kingdom, Research School of Biosciences, University of Kent at Canterbury, Canterbury, Kent CT2 7NJ, United Kingdom, and Inorganic Chemistry Laboratory, University of Oxford, South Parks Road, Oxford OX1 3QR, United Kingdom

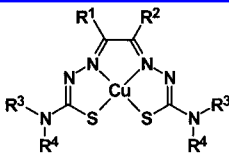
Received September 5, 2001

Copper diacetyl-bis(*N*⁴-methylthiosemicarbazone), Cu(II)ATSM, is a promising agent for imaging hypoxic tissue. Here we present results that provide insight into the chemical and electronic properties underlying previously observed structure–activity relationships. Density functional theory (DFT) calculations on the electronic structures and molecular orbitals of a series of 13 Cu(II)bis(thiosemicarbazone) analogues with different alkylation patterns and with fixed geometries based on the known structure of Cu(II)PTSM showed that the LUMO and the next lowest orbital were very close in energy, and their energy order was strikingly dependent on the ligand alkylation pattern in a way that correlated with hypoxia-selectivity and redox potentials. The LUMOs of Cu(II)ATSM and other hypoxia-selective analogues were predominantly *metal-based* (leading to a singlet reduced species) while the LUMOs of Cu(II)PTSM and other nonselective analogues were predominantly *ligand-based* (leading to a triplet reduced species). Upon relaxation of the geometric constraint and full optimization in both Cu(II)ATSM and Cu(II)GTS, the metal-based orbital became the LUMO, and the singlet was the thermodynamically preferred form of the reduced species. Chemical and electrochemical investigation showed that all Cu(II) complexes were reducible, but Cu(I)PTSM and other nonselective analogues dissociated immediately upon reduction with release of ligand (detected by UV–vis) while Cu(I)ATSM and other hypoxia-selective analogues did not. Instead they were rapidly re-oxidized to the Cu(II) complex by molecular oxygen. The reversible electrochemical reduction of nonselective complexes Cu(II)PTSM and Cu(II)GTS became irreversible in the presence of weak acid, whereas that of Cu(II)ATSM was unaffected. In light of these results we present a model to explain the structure–activity relationships on the basis of electronic structure and molecular vibrations.

Introduction

The search for radionuclide agents to image hypoxic tissues, for example in oncological, neurological, and cardiological applications, has recently turned to the use of copper complexes. Several copper radionuclides are available for both positron emission tomography (PET) (⁶⁰Cu, ⁶¹Cu, ⁶²Cu, and ⁶⁴Cu) and targeted therapy (⁶⁷Cu and ⁶⁴Cu).¹ The bis(thiosemicarbazone) complexes of copper (Chart 1) have shown special promise as radiopharmaceuticals, as illustrated by the perfusion imaging agent Cu(II)PTSM^{2,3} and the prototype hypoxia imaging agent Cu(II)ATSM.^{4–8} The latter was developed through rational design⁴ from a consideration of the mechanism by which Cu(II)PTSM^{9,10} and related complexes (e.g., Cu(II)KTS^{11,12}) are efficiently trapped in cells. It is accepted that bioreduction of copper(II) to copper(I) by intracellular reducing agents is at the heart of this mechanism, forming an unstable Cu(I) complex.⁹ This then dissociates to liberate the free ligand, whereupon the copper becomes bound to intracellular mac-

Chart 1. Nomenclature for the Copper Bis(thiosemicarbazone) Complexes

				
	R ¹	R ²	R ³	R ⁴
GTS	H	H	H	H
GTSM	H	H	CH ₃	H
PTS	CH ₃	H	H	H
PTSM	CH ₃	H	CH ₃	H
PTSM ₂	CH ₃	H	CH ₃	CH ₃
PTSE	CH ₃	H	C ₂ H ₅	H
PTSP	CH ₃	H	C ₆ H ₅	H
ATS	CH ₃	CH ₃	H	H
ATSM	CH ₃	CH ₃	CH ₃	H
CTS	C ₂ H ₅	CH ₃	H	H
CTSM	C ₂ H ₅	CH ₃	CH ₃	H
DTS	C ₂ H ₅	C ₂ H ₅	H	H
DTSM	C ₂ H ₅	C ₂ H ₅	CH ₃	H

* To whom correspondence should be addressed. C.A.R.: telephone, +44 1206 872540; fax, +44 1206 872592; e-mail, C.A.Reynolds@essex.ac.uk. J.R.D.: telephone, +44 1865 272639; fax, +44 1865 272690; e-mail, Jon.Dilworth@chem.ox.ac.uk. P.J.B.: telephone, +44 1227 823475; fax, +44 1227 763912; e-mail, P.J.Blower@ukc.ac.uk.

[†] University of Essex.

[‡] University of Kent at Canterbury.

[§] University of Oxford.

romolecules.¹⁰ It was suggested^{1,4} that lowering the reduction potential (i.e., making it harder to reduce), for example by altering the alkyl substituents on the PTSM ligand, would prevent trapping in less reducing (i.e., well-oxygenated) cells, leading to hypoxia-selective uptake.

In vitro experiments on a series of Cu(II)PTSM analogues (Chart 1) with varying Cu(II/I) reduction potentials^{7,13,14} not only demonstrated that hypoxia-selective uptake is possible (indeed, Cu(II)ATSM is currently under clinical evaluation for hypoxia imaging⁷)^{15–17} but also uncovered striking structure–activity relationships within the series. For example, bis(thiosemicarbazone) complexes with two alkyl groups at R1 and R2 (e.g., Cu(II)ATSM) are more selective for hypoxic cells in vitro and have markedly lower redox potentials than complexes with less than two alkyl groups at these positions (e.g., Cu(II)PTSM, Chart 1). On the other hand, addition of alkyl groups at the terminal positions (R3–R6) did not induce either a marked shift of redox potential or a significant increase in hypoxia selectivity.^{7,14} It was also observed that trapping of hypoxia selective complexes within hypoxic cells was partially reversible, whereas trapping of nonselective complexes was irreversible.⁷

Fujibayashi and co-workers suggest that the hypoxia-selectivity of Cu(II)ATSM compared to Cu(II)PTSM and Cu(II)KTS is accounted for by its considerably lower Cu(II/I) redox potential.⁴ The relevant intracellular reducing agent has been variously identified as complex I of mitochondrial electron transport chain in nontumor tissue, NADH-cytochrome b5 reductase or NADPH cytochrome P450 reductase in tumor tissue, or intracellular thiols such as glutathione.^{4,12,18,19} In accordance with this model, Cu(II)ATSM was reduced less efficiently than CuPTSM by submitochondrial particles, unless much larger amounts of NADH were added to shift the effective operating redox potential of the enzyme, presumably mimicking the effect of lack of intracellular oxygen.⁴ This allows more time for Cu(II)ATSM to escape from the cell, whereas Cu(II)PTSM and Cu(II)KTS undergo rapid reduction and dissociation even in the presence of oxygen. This hypothesis implicitly assumes that the reduced complexes dissociate rapidly whether they are hypoxia selective or not and so does not explain why the trapping of Cu(II)ATSM and Cu(II)ATS is at least partially reversible, whereas the trapping of Cu(II)PTSM and other nonselective analogues is irreversible.⁷ To account for this, it was suggested that the rates of dissociation and reoxidation of the reduced complexes, as well as the rate of reduction, assume an important role in the hypoxia-selectivity of the complexes.⁷ This possibility is not precluded by the experiments of Fujibayashi and co-workers because they were performed on tissue homogenates and subcellular fractions of tissues without the explicit exclusion of oxygen.⁴

To date, molecular modeling has not been used extensively within the radiopharmaceutical field (see references 20 and 21). Reichert has shown how molecular mechanics can be parametrized to reproduce structural properties of relevant copper(II) complexes,²⁰ but here our interest is primarily in the redox properties and so density functional theory offers a more appropriate method. Thus, to investigate further the chemical and electronic properties that underlie the observed structure–activity relationships, we have investigated the electrochemical and chemical reduction of the complexes and the ensuing chemistry, both computationally using density functional theory (DFT) and

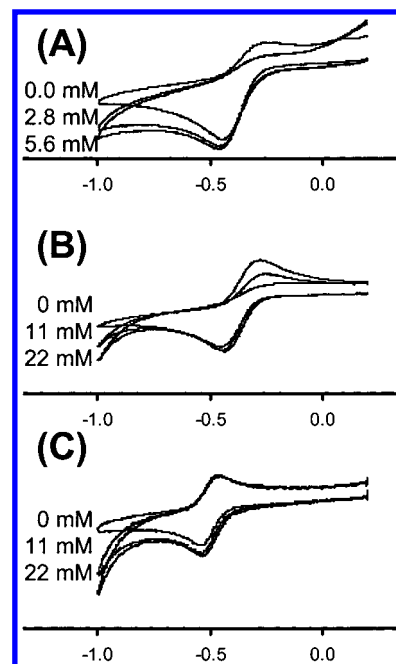
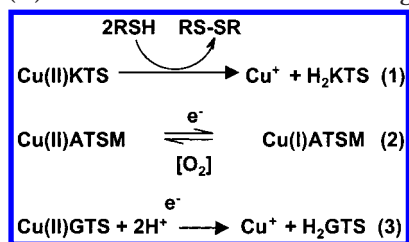


Figure 1. Cyclic voltammograms at different concentrations of acid: (A) CuGTS in the presence of acid, (B) CuPTSM in the presence of acid, and (C) CuATSM in the presence of acid. The figure shows that CuGTS is sensitive to relatively low concentrations of acid, that higher concentrations of acid are required to render the Cu(II)PTSM/Cu(I)PTSM couple irreversible, and that the CuATSM couple remains reversible even at the higher concentrations of acid.

experimentally. This study does not address the identity of the intracellular reducing agents involved. Instead, we focus on the comparative electronic structure and redox behavior of the copper complexes themselves.

Experimental Results

Cyclic voltammetry and UV–vis spectroscopy were used to study both the chemical and electrochemical redox behavior of representative complexes Cu(II)-ATSM, Cu(II)ATS, Cu(II)PTSM, Cu(II)PTS, Cu(II)-GTS, and Cu(II)GTS under varying acetic acid and oxygen concentrations. Previously, cyclic voltammograms of all of the complexes in this series have been reported to show a reversible Cu(II/I) redox couple, except that of Cu(II)GTS which was not fully reversible.^{7,14} Likewise, in our hands Cu(II)GTS showed a quasi-reversible couple in which the anodic current corresponding to reoxidation of the reduced complex was smaller than the cathodic current. This behavior suggests that the GTS complex undergoes further rapid reaction upon reduction, unlike the backbone-alkylated complexes for which we observed reversible couples. After the addition of varying concentrations of acetic acid, the Cu(II/I) couple for Cu(II)GTS became still less reversible, and the oxidative wave completely disappeared when the acetic acid concentration reached 5.6 mM (Figure 1a). On the other hand, the cyclic voltammogram of Cu(II)PTSM (Figure 1b) was much less sensitive to acid, requiring a far higher acetic acid concentration (22 mM) than Cu(II)GTS to yield a fully irreversible Cu(II/I) couple. The Cu(II/I) couple of Cu(II)ATSM remained fully reversible, even at the higher acetic acid concentration of 22 mM (Figure 1c). While Cu(II)ATSM and Cu(II)GTS represented the

Scheme 1. Behavior of (a) Cu(II)KTS, (b) Cu(II)ATSM, and (c) Cu(II)GTS in the Presence of Reducing Agents

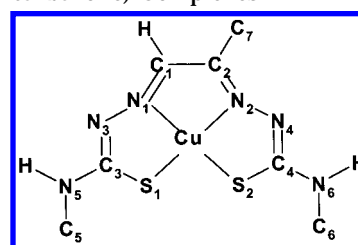
extremes of the range of behavior, qualitatively similar results were observed for the other complexes, that is, Cu(II)ATS behaved like Cu(II)ATSM, Cu(II)PTS behaved like Cu(II)PTSM, and Cu(II)GTS behaved like Cu(II)GTS (results not shown). The implications of these studies are that reduced Cu(II)GTS decomposes irreversibly on reduction, to some extent in the absence of added acid but particularly in its presence, and so Cu(I)GTS is unavailable for reoxidation whereas CuATSM is not irreversibly affected, even at relatively high concentrations of acetic acid in DMSO. (We note that that acetic acid is a very weak acid in DMSO—this is therefore a convenient way of adding low concentrations of acid. The CV of both types of complex becomes totally irreversible in the presence of small amounts of aqueous HCl. The lack of water solubility precluded a proper study of the pH dependence of the redox chemistry.)

The reactions of the copper(II) complexes with chemical reducing agents, and their subsequent reactivity with protons and oxygen, was investigated by in situ UV-vis spectrometry to characterize further the reversibility of reduction. The red DMSO solution of Cu(II)GTS gave rise to a distinct visible absorption at 497 nm ($\epsilon = 6227 \text{ cm}^{-1} \text{ M}^{-1}$). Addition of the reductant SnCl_2 did not alter this spectrum, but upon addition of acetic acid (45 mM) as well as SnCl_2 , the absorption immediately disappeared and a pale yellow solution was formed with a distinct absorption at 373 nm ($\epsilon = 5467 \text{ cm}^{-1} \text{ M}^{-1}$) corresponding to the free ligand H_2GTS . Similar behavior was observed with powdered zinc in place of SnCl_2 . No color change was observed when acetic acid was added to the Cu(II)GTS solution without the reductant. The results were the same when the experiments were repeated under anaerobic conditions. In contrast, Cu(II)ATSM showed an absorption at 475 nm ($\epsilon = 7951 \text{ cm}^{-1} \text{ M}^{-1}$) which remained unchanged on addition of SnCl_2 and acetic acid, presumably because of the lower reduction potential of Cu(II)ATSM. Upon the addition of a stronger reducing agent, sodium naphthalide, without acid and in the presence of air, the orange solution of Cu(II)ATSM changed to a pale yellow color. The electronic spectrum of this solution was featureless in the visible range and lacked the absorption shoulder at 367 nm ($\epsilon = 6552 \text{ cm}^{-1} \text{ M}^{-1}$) characteristic of H_2ATSM , and hence it did *not* contain free ligand. The addition of acetic acid did not alter the spectrum. The yellow species remained indefinitely under anaerobic conditions, but on standing for 30 s in air, the original orange color (corresponding to Cu(II)ATSM) returned, and the original spectrum was restored. A summary of these reactions can be seen in Scheme 1.

Table 1. Comparison of Selected Bond Lengths for Optimized Structures of Cu(II)PTSM at the Local (LSD) and Nonlocal (NLSD) Levels of Theory and of the Crystal Structure (crystal)^{47 a}

bond length/Å	LSD	NLSD	crystal
Cu1–S1	2.204	2.332	2.259(1)
Cu1–S2	2.209	2.325	2.269(1)
Cu1–N1	1.954	2.052	1.977(4)
Cu1–N2	1.942	2.052	1.965(3)
S2–C4	1.748	1.786	1.776(4)
N4–C4	1.331	1.349	1.315(5)
N2–N4	1.334	1.363	1.367(6)
N5–C2	1.316	1.325	1.300(5)
C1–C2	1.440	1.462	1.452(7)
C1–N1	1.308	1.319	1.289(4)
N1–N3	1.328	1.352	1.345(5)
N3–C3	1.335	1.347	1.337(4)
C3–S1	1.745	1.784	1.741(5)

^a Numbering is from Chart 2.

Chart 2. Numbering Scheme for Copper Bis(thiosemicarbazone) Complexes

Computational Results

To assess the value of the density functional theory (DFT) methods in studying these complexes while minimizing costs in CPU time, we compared the experimental, local spin density (LSD), and nonlocal spin density (NLSD) geometries of Cu(II)PTSM. The results for the bond lengths, given in Table 1, show that both methods work well. The planarity of the crystal structure is maintained in both optimized geometries. The LSD geometry, however, consistently underestimates the bond lengths while the NLSD method overestimates the bond lengths, generally to a slightly greater extent. However, the difference in bond length between C4–N4 and N4–N2 (using numbering in Chart 2) is reproduced in the NLSD structure but not in the LSD structure. Thus, overall the key geometric features of Cu(II)PTSM are reproduced slightly more adequately using NLSD methods.

The effect of introducing alkyl groups at positions R1 to R6 on the electronic structure of the copper(II) complexes was investigated computationally using the Cu(II)PTSM template geometry. The spin orbitals of key significance for the reduction of the Cu(II) complexes are the lowest unoccupied molecular orbitals (LUMOs). Figure 2 shows the shape of the highest occupied molecular orbital (HOMO) α_1 and the next three unoccupied orbitals above it, β_1 , α_2 , and β_2 . The HOMO α_1 is a σ -orbital lying in the plane of the complex. It has a large $dx^2 - y^2$ component and is metal–ligand antibonding in character. Spin orbital β_1 is spatially similar (the α_1 and β_1 orbitals are identical in a restricted formalism). Spin orbitals α_2 and β_2 are almost exclusively ligand-based and are part of a highly conjugated π -system extending across the entire ligand.

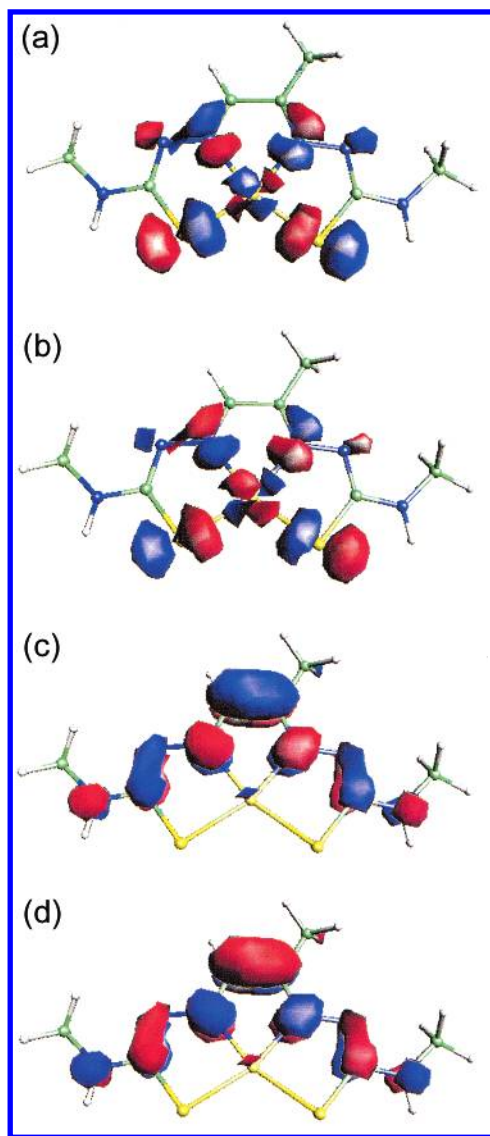


Figure 2. Molecular orbital pictures of Cu(II)PTSM. Orbital 1 is primarily metal-based; orbital 2 is primarily ligand-based. Part a is the $\alpha 1$ orbital, i.e., the HOMO; part b is the $\beta 1$ orbital, i.e., the LUMO + 1; part c is the $\alpha 2$ orbital, i.e., the LUMO; and part d is the $\beta 2$ orbital, i.e., the LUMO + 3.

The calculated shapes of all four orbitals are almost unaffected by addition of alkyl groups at R1–R6 across the series.

The calculated energies of $\alpha 1$, $\beta 1$, $\alpha 2$, and $\beta 2$ are listed in Table 2. All four of these orbitals are very close in energy. In particular, $\alpha 2$ and $\beta 1$ (the two lowest unoccupied orbitals) are never more than 0.03 eV apart. This makes the energy order of $\alpha 2$ and $\beta 1$ extremely sensitive to influences such as alkylation and geometry. Both $\alpha 2$ and $\beta 1$ are raised in energy by successive alkylation at R1–R6. However, it is noticeable that alkylation at R1 and R2 raises the energy of $\alpha 2$ slightly more than that of $\beta 1$. Consequently, while $\alpha 2$ (ligand-based) is the LUMO when R1 = R2 = H, $\beta 1$ (metal-based) is the LUMO when R1 = R2 = alkyl (Figure 3). In contrast, alkylation of the N-terminal sites R3–R6 raises the $\alpha 2$ and $\beta 1$ energies by the same amount and does not change the energy order. The character of the HOMO ($\alpha 1$) is invariant across the series, consistent with the close similarity of all the EPR spectra of the complexes.⁷

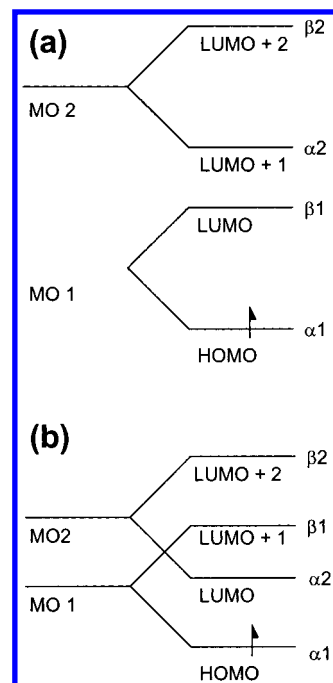
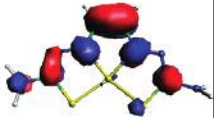

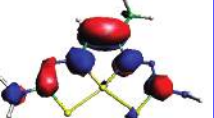
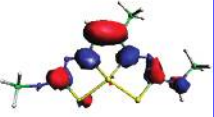
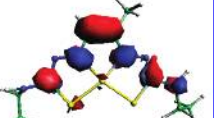
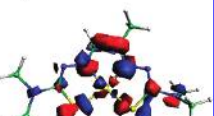
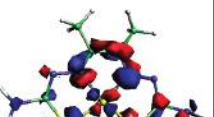
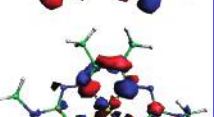
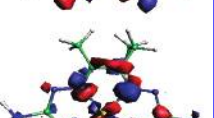
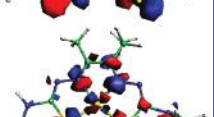
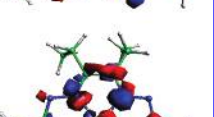
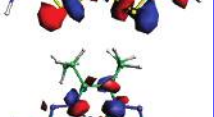


Figure 3. Molecular orbital energy diagram showing the two different relative orderings of the HOMO and LUMO of the copper(II) complexes. Part a applies to complexes where the $\beta 1$ spin-orbital is lower in energy than the $\alpha 2$ spin-orbital; thus $\beta 1$ is the LUMO. Part b applies to complexes where the $\beta 1$ spin-orbital is greater in energy than the $\alpha 2$ spin-orbital; thus $\alpha 2$ is the LUMO. α and β refer to the different spins.

In the calculations above, the changes in electronic structure were constrained to the geometry of the Cu(II)PTSM template. Full optimization with relaxation of this constraint was performed on three complexes: Cu(II)PTSM plus Cu(II)ATSM and Cu(II)GTS, which represent the extremes of redox potential and hypoxia selectivity. The new optimized geometries are given as Supporting Information; the main difference is the increase in the backbone C–C bond length with increasing methylation at R1 and R2 from 1.455 Å (in GTS) to 1.462 Å (in PTSM) to 1.481 Å (in ATSM).


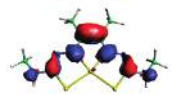
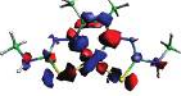
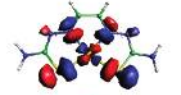
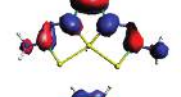
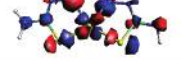
Despite minor geometric changes, the shapes of the $\alpha 1$, $\beta 1$, $\alpha 2$, and $\beta 2$ orbitals were essentially unchanged by full optimization. However, the reversal of the ordering of the $\beta 1$ and $\alpha 2$ orbital energies caused by alkylation in the nonoptimized series was no longer evident, and $\beta 1$ was the LUMO for both ATSM and GTS (Table 3). This result was confirmed by calculations employing different functionals (PW91, HCTH—results not shown). However, differences are seen in the calculated harmonic frequencies for ATSM and GTS, given as Supporting Information. The additional methyl groups introduce many more molecular vibrations in Cu(II)-ATSM. Indeed, the number of vibrations calculated between 0 and 1600 cm^{-1} is almost double that of Cu(II)GTS. Contributions to a calculated molecular vibration that distorts the copper coordination geometry are commonplace, particularly below 400 cm^{-1} . The intensities, and thus the relative populations, of these vibrations are of a comparable level to other vibrations in the calculated spectrum. Cu(II)GTS however, shows extremely few vibrations that distort the copper coordination, especially below 400 cm^{-1} , and these are

Table 2. Orbital Energies of Cu(II)PTSM Analogues Calculated Using the PTSM Template^a

Complex	R1,R2	R3,R4	E(obs)	$\alpha 1$	$\beta 1$	$\alpha 2$	$\beta 2$	LUMO orbital
GTS	H, H	H, H	-0.428	-4.14	-3.62	-3.64	-3.52	
GTSM	H, H	Me, H	-0.429	-4.02	-3.51	-3.53	-3.41	
PTS	H, Me	H, H	-0.502	-4.03	-3.45	-3.45	-3.39	
PTSM	H, Me	Me, H	-0.510	-3.94	-3.42	-3.43	-3.33	
PTSE	H, Me	Eth, H	-0.524	-3.92	-3.39	-3.41	-3.30	
PTSM ₂	H,	Me, Me	-0.527	-3.82	-3.28	-3.27	-3.20	
ATS	Me, Me	H, H	-0.587	-3.94	-3.35	-3.32	-3.25	
ATSM	Me, Me	Me, H	-0.590	-3.84	-3.26	-3.24	-3.18	
CTS	Me, Eth	H, H	-0.590	-3.91	-3.32	-3.29	-3.24	
CTSM	Me, Eth	Me, H	-0.583	-3.81	-3.23	-3.21	-3.15	
DTS	Eth, Eth	H, H	-0.585	-3.90	-3.31	-3.29	-3.24	
DTSM	Eth, Eth	Me, H	-0.577	-3.81	-3.23	-3.20	-3.15	

^a Orbital energies are in electron volts. The R group numbering is taken from Chart 1. The redox potential, $E(\text{obs})$, is in volts. The energy of the LUMO is given in bold.

Table 3. Calculated Gas-Phase Molecular and Orbital Energies Using BLYP Functional at Full Optimization^a

Complex	SCF energy	$\alpha 1$	$\beta 1$	$\alpha 2$	$\beta 2$	LUMO for Cu(II) / HOMO for Cu(I)
<i>ATSM</i>						
Cu(II)	-1 931 344.00	-4.10	-3.46	-2.72	-2.68	
Cu(I) Triplet	-1 931 367.10	-0.13	0.56	0.76	1.24	
Cu(I) Singlet	-1 931 383.27	-0.03		1.40		
<i>GTS</i>						
Cu(II)	-1 832 727.01	-4.47	-3.84	-3.17	-3.12	
Cu(I) Triplet	-1 832 757.66	-0.67	-0.45	-0.26	0.44	
Cu(I) Singlet	-1 832 772.78	-0.17		1.20		

^a SCF energies are in kcal mol⁻¹; orbital energies are in electron volts. The energies of the LUMO for Cu(II) and HOMO for Cu(I) are depicted in bold.

Table 4. Effect on the $\alpha 2/\beta 1$ Energy Gap of Substituents with Differing Electron Donating/Withdrawing Power at the R2 Position in Cu(II)PTSM

	group	LUMO	gap/eV
increasing electron donation ↑	-NH ₂	$\beta 1$	0.100
	-OH	$\beta 1$	0.015
	- <i>tert</i> -butyl	$\alpha 2$	-0.007
	-methyl	$\alpha 2$	-0.003
	-H	$\alpha 2$	-0.020
increasing electron withdrawl ↓	-Cl	$\beta 1$	0.002
	-I	$\beta 1$	0.024
	-CN	$\alpha 2$	-0.034

considerably smaller in intensity than other vibrations.

Calculations on the expected effect of different electron donating R1 and R2 groups on the nature of LUMO in a number of hypothetical Cu(II) bis(thiosemicarbazone) analogues (constrained to the Cu(II)PTSM template geometry) were performed. The results are summarized in Table 4. They indicate that the largest difference between the metal based LUMO, $\beta 1$, and the ligand-based LUMO + 1, $\alpha 2$, is expected when R is the strongest π -electron donor, in this case -NH₂.

The effect of acid on the reduced complexes was found experimentally to be a major discriminator between ATSM and GTS. Consequently, we have calculated the protonation energies for Cu(I)ATSM⁻ and Cu(I)GTS⁻ (Table 5) and have shown that N3/N4 is the preferred protonation position, in both the gas phase and in aqueous solution—at least for monoprotection of the monomer. The electrostatic potentials for the singlet Cu(I) anions are very similar, suggesting that the chemistry is likely to be similar, with the gas-phase energies showing that singlet Cu(I)ATSM⁻ is more readily pro-

Table 5. Comparison of Energies, in kcal mol⁻¹, for Protonated Species of Cu(I)ATSM and Cu(I)PTSM^a

protonation site	QM	ΔG_{hyd}	total energy
Cu(I)ATSM			
N3/4	-1 931 791.78	-17.09	-1 931 808.87
N5/6	-1 931 772.42	-25.23	-1 931 797.65
S1/2	-1 931 781.48	-17.59	-1 931 799.07
Cu(I)GTS			
N3/4	-1 833 121.11	-18.64	-1 833 139.75
N5/6	-1 833 100.73	-30.93	-1 833 131.66
S1/2	-1 833 109.05	-16.35	-1 833 125.40

^a The lowest total energy is shown in bold.

tonated than singlet Cu(I)GTS⁻. This contrasts with the higher observed reactivity of the GTS complex. The electrostatic potential plots of the Cu(I)ATSMH and Cu(I)GTSH compounds protonated at N3, N6, and S1 are also similar, but they do show that Cu(I)GTSH is likely to be protonated more readily (at N3/N4 and S1/S2) in a diprotonated species. There are no significant differences in the bond lengths between Cu(I)ATSM⁻ and Cu(I)GTS⁻ or between protonated Cu(I)ATSM⁻ and protonated Cu(I)GTS⁻. These results are given as Supporting Information and are not discussed below.

Discussion

The density functional calculations have addressed four properties relevant to bithiosemicarbazone chemistry, namely structure (through geometry optimization), vibration (through harmonic frequency calculations), protonation (through electrostatic potential and energetic calculations), and reduction (through orbital diagrams and energetic calculations). The stability of

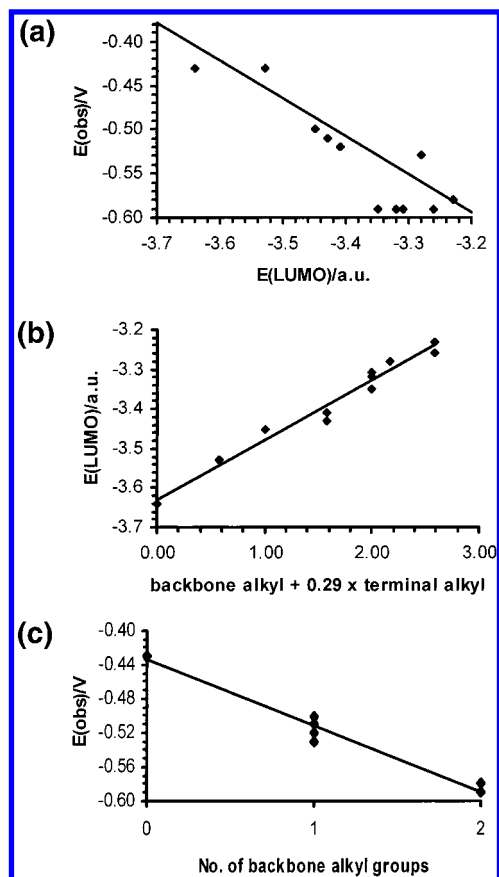


Figure 4. Linear relationships between (a) the redox potential and the LUMO energy, (b) the LUMO energy and the number of alkyl groups (weighted according to position), and (c) the redox potential and the number of backbone alkyl groups.

the complexes depends on the degree of conjugation, and in this respect, it was considered that the nonlocal density functional calculations were superior to the local calculations as they gave a better reproduction of the alternation of ring bond lengths. The nonlocal absolute errors were slightly higher than those obtained with the local spin density method and greater than would normally be expected for organic compounds. Nevertheless, the agreement is within the range normally expected for transition metal complexes—for example, see references 22–28—and this gives confidence in the results.

Similar confidence may be obtained from the link between the orbital energies and redox properties. The calculated orbital energies of the series of analogues at the PTSM template geometry are consistent with previously observed trends in Cu(II/I) redox potential.^{7,14,29} A major contributing factor to a low redox potential (i.e., a “difficult” reduction process) is a high energy LUMO and indeed here there is a good linear relationship—see Figure 4a and eq 1. This is a strong correlation compared to that observed in other systems such as nitroimidazoles (see, for example, reference 30). We note that as alkyl groups are added to the ligand, the calculated LUMO energy increases and the Cu(II/I) redox potential becomes more negative (Table 2). The direct correlation between the total number of alkyl groups and the LUMO energy is poor because backbone alkylation at R1 or R2 caused a much greater effect (about 3.5 times—see eq 2, which is plotted in Figure 4b in the simplified form of eq 3) than alkylation at the

terminal positions R3–R6.

$$E_{\text{obs}} = -0.43(\pm 0.07)E_{\text{LUMO}} - 1.97(\pm 0.23) \quad (1)$$

$$R^2 = 0.80, F = 41, n = 12, \sigma = 0.028$$

$$E_{\text{LUMO}} = 0.15(\pm 0.09)B + 0.04(\pm 0.05)T - 3.63(\pm 0.02) \quad (2)$$

$$R^2 = 0.99, F = 155, n = 12, \sigma = 0.023$$

$$E_{\text{LUMO}} = 0.15(\pm 0.09)(B + 0.292T) - 3.63(\pm 0.02) \quad (3)$$

$$R^2 = 0.97, F = 344, n = 12, \sigma = 0.022$$

$$E_{\text{obs}} = -0.077(\pm 0.003)B - 0.003(\pm 0.002)T - 0.429(\pm 0.005) \quad (4)$$

$$R^2 = 0.97, F = 344, n = 12, \sigma = 0.0077$$

$$E_{\text{obs}} = -0.077(\pm 0.003)B - 0.434(\pm 0.005) \quad (5)$$

$$R^2 = 0.97, F = 540, n = 12, \sigma = 0.0085$$

Here, E_{obs} is the experimental redox potential, E_{LUMO} is the LUMO energy, B and T are the number of backbone and terminal alkyl groups respectively, and R^2 , F , n , and σ are the correlation coefficient squared, the F -value, the number of data points, and the standard deviation, respectively.

The link between redox potential and the number of added alkyl groups is complex, since the effect of the backbone alkyl groups is approximately 24 times that of the terminal alkyl groups and indeed the t -value for the term in T in eq 4 is 1.8, suggesting that terminal alkylation is not really significant, hence eq 5, Figure 4c, gives a better relationship between redox potential and alkylation. These correlations must be viewed in the context of the limitations. The calculations were performed at the template rather than optimized geometries and omitted several factors including the energy of the Cu(I) species, the solvation free energy, and other enthalpy and entropy contributions.^{31,32} The different forms of eqs 2 and 5 suggest that the effects of terminal alkylation on the redox potential are counterbalanced by corresponding effects on solvation and the energy of the Cu(I) species. However, the backbone alkyl groups do have a distinct effect. Moreover, we note that the midpoint of the oxidation/reduction peak⁷ does not necessarily correspond to a thermodynamic electrode potential, and this may weaken the correlations. Nevertheless, these correlations involving the orbital energies, degree of alkylation, and the observed electrochemical potentials reinforces the usefulness of these computational models.

Encouraged by this, we examined the spatial nature of the frontier orbitals in relation to alkylation pattern. An unusual feature of this series of complexes is that in every case the LUMO is not isolated but is accompanied by another spin orbital that is very close in energy but very different spatially. The reversal of the energy order of these orbitals midway through the series (Figure 3) means that the complexes with two backbone alkyl groups have β_1 as the LUMO while complexes without backbone alkyl groups have α_2 as the LUMO. Thus, other factors being equal, on energetic grounds

one might expect reduction of Cu(II)ATSM to populate the β_1 orbital, giving rise to a singlet, closed shell Cu(I) d^{10} species, while at the other extreme, reduction of Cu(II)GTS should populate α_2 giving rise to a triplet species with an unpaired electron localized primarily on the ligand (see Table 2). Since the ligand-based α_2 orbital has a distinctly different spatial character to the β_1 orbital, it is likely to give rise to different chemistry, particularly as the triplet is expected to be more reactive than the singlet. Alternative locations for an electron to give multiple-spin states have been noticed elsewhere, both in copper complexes³³ and in metalloporphyrins.³⁴ The reduced form of CuGTS might thus be less stable than the reduced form of CuATSM, either because of its unpaired electrons or because the additional ligand-based electron renders the ligand more basic and hence vulnerable to acid-catalyzed dissociation.

These results provide a stimulus for further experimentation to look for chemical differences between members of the series. Cu(II)ATSM shows a fully reversible Cu(II/I) couple even in 22 mM acetic acid, while at the other extreme Cu(II)GTS is not completely reversible even when no acid is added (adventitious protons from traces of water may be responsible for this), while the behavior of Cu(II)PTSM is intermediate between these two. This is consistent with the idea that double alkylation (R1/R2) protects the reduced complex against acid-induced dissociation by ensuring that the additional electron is more metal-based rather than primarily ligand-based (see Table 2). Monitoring the chemical reduction process by UV spectroscopy lends support to the assumption that the irreversibility in reduction of Cu(II)GTS is due to ligand dissociation, since free ligand was detected upon reduction in the presence of protons. In contrast, no free ligand was detected on reduction of Cu(II)ATSM, and the putative [Cu(I)ATSM]⁻ anion, instead of dissociating, was readily reoxidized to Cu(II)ATSM (either electrochemically or by molecular oxygen). Of the complexes investigated in this way, the least alkylated complex was both the most easily reduced biologically, as determined by the measured redox potential and the LUMO energy calculations, and the most rapidly dissociated in the presence of acid.

These calculations and experiments demonstrate that the trends in the chemical and electrochemical behavior within the series provide a chemical rationale for the trapping mechanism suggested on the basis of the cell uptake and washout experiments.⁷ Combining the present results with the *in vitro* biological results of both Fujibayashi et al.⁴ and Dearling et al.,⁷ we offer the following model to explain the different biological behavior of Cu(II)PTSM and Cu(II)ATSM. Both complexes are bio-reduced, although presumably Cu(II)ATSM is bio-reduced less efficiently. Once reduced, intermediate species such as [CuATSM]⁻ and [CuPTSM]⁻ are trapped within the cell because of their charge. (Nominally, this is a negative charge but extensive protonation of the anions could also lead to trapping of positive species.) They can then follow one of two competing pathways: reoxidation to the uncharged Cu(II) species (which can escape by diffusion), or proton-induced dissociation (which releases copper to be irreversibly sequestered by intracellular proteins). [CuPTSM]⁻ favors the dissociation route because it is hard to reoxidize but readily

protonated and dissociated, while [CuATSM]⁻ favors the reoxidation route because it is easily oxidized but chemically more resistant to protonation. Thus, copper is irreversibly trapped from Cu(II)PTSM irrespective of oxygen concentration, so Cu(II)PTSM is not hypoxia-selective. On the other hand, copper from Cu(II)ATSM is trapped reversibly as [CuATSM]⁻ (if oxygen is absent), with the possibility of irreversible trapping by dissociation over a longer period. Cu(II)ATSM is thus hypoxia-selective. The chemical and electrochemical experiments confirm that CuATSM in its reduced form is resistant to acid-catalyzed dissociation (in the presence of a weak acid), whereas reduced CuPTSM and CuGTS are not, and the calculations suggest that an electronic origin (singlet versus triplet) may explain this difference.

The foregoing discussion provides a plausible rationale for the relationship between structure and both redox potential and hypoxia-selectivity. However, the limitations already raised suggest that caution should be exercised in their interpretation. The α_2 - β_1 energy gap (<0.03 eV) is very small compared to the shifts in absolute energy caused by alkylation and, were it not for the consistency with which they follow the backbone alkylation pattern, might be dismissed as insignificant. Moreover, in the absence of more X-ray crystal structure information, the accuracy with which the CuPTSM template geometry models each member of the series remains unknown. Alkylation causes electronic changes that might manifest themselves in altered geometry of the metal coordination sphere. When full optimization was allowed for Cu(II)ATSM and Cu(II)GTS, the Cu(II) complexes remained essentially planar with the largest changes occurring in the backbone C-C bond length: to 1.455 Å for CuGTS, and to 1.481 Å for CuATSM. These changes are mirrored in X-ray structures (results to be published). However, this small change led to a small but significant increase in the α_2/β_1 energy gap ensuring that β_1 remained lower than α_2 in both cases. Also, optimization of the reduced Cu(I) species suggests that, again at both extremes of the series, the optimized singlet state has lower energy than the optimized triplet state (see Table 3). These observations raise a serious objection to the singlet-triplet model: the singlet is lower in energy than the triplet at both extremes of the series, so on energy grounds there may be no need to invoke a triplet reduced state at all. However, attempts to explain the chemical differences based solely on singlet properties also have difficulties. The molecular electrostatic potential plots for the thermodynamically preferred singlet states of the reduced anions show no qualitative differences between the ATSM and GTS complexes that could explain the chemical and electrochemical observations. Moreover, the quantum mechanical energies of the Cu(I) singlet anions and their protonated forms suggest that the ATSM species is *more* basic than the GTS species (see Supporting Information).

These conflicting results raise a dilemma since the seemingly more thorough calculations presented in Table 3 remove the plausible explanation, suggested by the Cu(II)PTSM template geometry calculations, for the real and significant experimental differences between the complexes. However, these conflicting results do

suggest that in the essentially planar Cu(II) complexes, the energy ordering of the α_2 and β_1 is extremely sensitive to even small changes in geometry, which may perhaps be accessible within the ambient temperature vibrational amplitudes. One must therefore still entertain the possibility that upon reduction the additional electron may populate either α_2 or β_1 , particularly as the difference in energy between fully optimized singlet and triplet Cu(I) is only about 15 kcal mol⁻¹ (Table 3). The calculations on the singlet and triplet use different methodologies (restricted and unrestricted Kohn Sham theory). This means that the energies are not directly comparable (and so the triplet Cu(I)GTS may actually be lower in energy than singlet Cu(I)GTS). However, the conclusion that this difference is very small is significant and is unusual for such complexes. The calculations at the PTSM template geometry suggest that on orbital energy grounds alone, planar Cu(II)GTS will be about 8-fold more likely than planar Cu(II)ATSM to follow the α_2 route on reduction. This raises the possibility that on reduction Cu(II)GTS forms a triplet complex, rather than the more stable singlet, for kinetic rather than thermodynamic reasons. In other words, it may be the nature of the LUMO in the Cu(II) complex, not the thermodynamic preference in the reduced state for singlet or triplet, that determines whether a singlet or a triplet is initially formed.

The calculated geometry of singlet Cu(I) d¹⁰ complexes is distorted tetrahedral—resulting from the increased effective radius of the copper and a greater antibonding nature in the ligand-to-metal bonds. The triplet reduced complexes, however, are perfectly planar, mimicking the geometry of the oxidized Cu(II) complexes. A study of the calculated vibrational modes of Cu(II)ATSM shows a number of low energy out-of-plane vibrational modes that result in loss of planarity. The modes are the result of additional coupled vibrations from the backbone and terminal methyl groups and are absent from the calculated vibrational modes of CuGTS (see Supporting Information). Their effects can be seen in a loose optimization of the Cu(II) complexes, starting from the distorted Cu(I) singlet geometries: the CuATSM geometry remains distorted, whereas the CuGTS geometry—which lacks the extra vibrational modes—becomes perfectly planar (results not shown). One may conclude that the extra vibrational modes in Cu(II)ATSM result in a greater flexibility of the Cu(II) complex, so that it may fluctuate through the planar geometry at room temperature and may be more distorted than the optimized geometry suggests. The Cu(II)ATSM is therefore more likely than Cu(II)GTS to form the distorted singlet complex on reduction for vibrational as well as electronic reasons.

The triplet hypothesis suggests two further ways of increasing selectivity that can be tested experimentally. First, by including a functional group with a greater number of out-of-plane bending modes, the flexibility of the planar system can be increased and the complex would be less likely to form the triplet on reduction. Second, by choosing a more electron donating functional group to incorporate at R1/R2, as well as lowering the redox potential, we may prohibit the formation of the triplet by donating electrons into the ligand-based α_2 orbital. In Cu(II)ATSM, the electron donation takes the

form of hyperconjugation, apparent in orbitals well below the HOMO, involving a C–H bond of the backbone alkyl group, but this interaction could be made stronger by replacing the alkyl group with an amino group in which the electron donor would be a nitrogen p-lone pair. Table 4 shows that the largest gap between α_2 and β_1 (with β_1 being the lower of the two) is seen with the most electron donating group, –NH₂. Bis-(thiosemicarbazone) ligands with a nitrogen atom at this location are known.³⁵

Summary

The chemical and electrochemical results support the hypothesis that intracellular reduction of the Cu(II) complexes can lead to two distinct patterns of chemical behavior: rapid acid catalyzed dissociation (nonhypoxia-selective complexes CuGTS, CuPTSM, etc.) or resistance to dissociation allowing subsequent reoxidation by molecular oxygen, if present (hypoxia-selective complexes, CuATSM, etc.). This hypothesis is consistent with the previously reported uptake-washout experiments. The calculations, within their obvious limitations, suggest that a possible rationale for which of the two behavior patterns is adopted is the relative likelihood of reduction to a *triplet* state with additional electron density on the ligand or to a *singlet* with additional electron density on the metal. Which of these two states is formed could be determined by both the electronic and vibrational consequences of incorporating alkyl groups at R1–R6. The energy order of two spatially distinct orbitals (α_2 , more metal-based, and β_1 , primarily ligand-based) was strikingly dependent on the ligand alkylation pattern in a way that correlated with hypoxia-selectivity and redox potentials. Even though we do not attach great weight to quantitative details of the calculations because of the numerous uncertainties, we have established trends within the series that cannot be ignored. An unusual property of these complexes that distinguishes them from other simple coordination complexes and perhaps underlies their remarkable biological properties is the presence of a very low-lying vacant spin orbital close in energy to the LUMO.

This model suggests avenues for further investigation of the mechanism that distinguishes hypoxia-selective complexes from nonselective ones. Spectroelectrochemical studies (EPR and UV–vis spectrometry at an electrode surface) could be used to attempt to identify the putative triplet states. Crystallographic studies of both Cu(II) complexes across the series and of any reduced complexes that can be isolated are required to determine the validity of the optimized geometries and help refine the calculations. While it is difficult to determine what one could measure *inside the cell* which would shed light on the nature of the reduced state, experiments are currently in progress to prepare water soluble bis-(thiosemicarbazone) complexes which would permit detailed redox studies in aqueous media. To determine whether delayed reaction of CuATSM following reduction is an important determinant of its hypoxia selectivity, biological studies should focus on the reversibility of uptake, and the speciation of the copper (especially of the copper released from the cell upon reoxygenation) as a function of the time of incubation under hypoxia. The proposed model also introduces the possibility that intracellular pH could affect the

retention of the complexes in tissues by controlling the rate of dissociation (or association) of the reduced complexes. This possibility, which is pertinent because hypoxic tissue can become acidified, remains to be investigated experimentally.

Materials and Methods

All experimental manipulations were performed with the exclusion of air, unless otherwise stated. ATSM, ATS, PTSM, PTS, GTSM, and GTS ligands and their copper complexes were prepared according to the literature methods.^{7,36} Glacial acetic acid, stannous chloride, zinc powder, and anhydrous dimethyl sulfoxide (DMSO) were purchased from Aldrich and used without further purification. Sodium naphthalide in dry tetrahydrofuran was freshly prepared by adding Na metal (1 equiv) in small pieces to a solution of naphthalene in dry tetrahydrofuran. Aliquots of the deep green solution were then used to provide 1 equiv of reductant. UV-vis spectra of DMSO solutions were recorded in quartz cells on a Cintra 10 (CGU) scanning spectrophotometer. Cyclic voltammetric investigations were performed on an EG&G model 362 scanning potentiostat using WinCV (Condecon, Version 1.0) data capture and analysis software. All cyclic voltammetry measurements were carried out under a dinitrogen atmosphere at a scan rate of 200 mV s⁻¹ using a glassy carbon working electrode, platinum auxiliary electrode, and silver wire reference electrode in still dry deoxygenated DMSO (15 mL) with 0.1 M [Bu₄N][BF₄] as support electrolyte and a sample concentration of 0.4 mM.

Variable Wavelength UV-Vis Experiments. UV-vis spectra were recorded (λ = 200 to 700 nm) of a 0.4 mM solution of a Cu(II) bis(thiosemicarbazone) complex in anhydrous DMSO (3 mL) in a quartz cell. Then an excess of SnCl₂·2H₂O (22.5 mg, 0.1 mM) and acetic acid (8 μ L, 45 mM) was added, and the cell was shaken vigorously for 30 s. Powdered zinc was used in place of stannous chloride in some experiments. Spectra were then recorded at 1 min intervals over 15 min. Control spectra of SnCl₂·2H₂O and acetic acid in anhydrous DMSO were also recorded.

Cyclic Voltammetry Experiments. Cyclic voltammograms, performed in anhydrous DMSO, were recorded, then re-recorded after addition of sequential aliquots of glacial acetic acid (2 \times 10 μ L to give concentrations of 11 and 22 mM in the case of Cu(II)PTSM and Cu(II)ATSM, and 2 \times 2.5 μ L to give concentrations of 2.8 and 5.6 mM in the case of Cu(II)GTS).

Computational Methodology. The quantum mechanical calculations were performed using density functional methods,³⁷ as implemented in the DGAUSS suite of programs through the UNICHEM graphical user interface.^{38,39} Generally, the calculations employed the nonlocal Becke'88 functional for exchange⁴⁰ and the Lee, Yang, and Parr functional for correlation⁴¹ (together denoted BLYP), but a variety of other functionals were also used, namely the nonlocal Perdew and Wang '91 functional for exchange and correlation (denoted PW91)⁴² and Handy's empirically fitted HCTH functional.⁴³ Local spin density calculations employed the local Vosko-Wilk-Nussair functional for correlation.⁴⁴ All the calculations used a DZVP (double- ζ plus valence polarization) basis set.⁴⁵ Loose optimization required that the maximum force on any degree of freedom be less than 5 \times 10⁻³ hartree bohr⁻¹; full optimization required that the maximum force on any degree of freedom be less than 5 \times 10⁻⁴ hartree bohr⁻¹. In their oxidized form, the copper complexes are all formally in the Cu(II) oxidation state (*d*⁹) (i.e., they possess an unpaired electron in the highest occupied molecular orbital (HOMO)). Consequently, the calculations on the doublet were carried out using the spin-unrestricted formalism.⁴⁶ There are two relevant consequences of this approximation: first the degeneracy between the α (spin up) and β (spin down) orbitals is lost, and second the energy of singlet and triplet species cannot be compared directly because their calculations involve different approximations.

To reduce the CPU requirements, the structure of Cu(II)-PTSM was initially optimized using local spin density calculations

that employed the local Vosko-Wilk-Nussair functional for correlation⁴⁴ as well as the nonlocal BLYP functional. The results were compared to the experimentally determined X-ray crystal structure.⁴⁷ Two approaches to geometry determination of the copper(II) complexes were followed. In the first approach, a loose optimization was carried out on the Cu(II)PTSM experimental structure⁴⁷ (the geometry was taken from the literature as the crystal structure has not been deposited with the Cambridge Crystallographic Database), and substituents were then added using standard geometries. This geometry, referred to as the *PTSM template geometry*, was used for single point calculations on all members of the family of Cu(II)-bis(thiosemicarbazone) analogues listed in Chart 1. This PTSM template geometry was chosen because its alkylation pattern and redox potential are intermediate between the extremes: it carries one backbone methyl group rather than two (ATSM) or none (GTS). It therefore gives the most appropriate common geometry for comparative calculations on the whole series of compounds. An additional advantage of using this structure is that it is related to experiment and can therefore function as a control for the calculations that employed optimized geometries. The second approach involved full optimization, at the nonlocal level, of the complexes at the extremes of the hypoxic selectivity and redox potential range, namely Cu(II)-ATSM and Cu(II)GTS, in addition to Cu(II)PTSM. The second derivatives were calculated at the final optimized geometry to obtain harmonic frequencies.³⁸

To gain insight into the electronic structure of the reduced copper complexes, the nature of the LUMO of the Cu(II) species was examined. Further explicit calculations on the reduced species were carried out using full optimization at the nonlocal level of theory, as described below, on both singlet and triplet forms.

Two approaches were followed to study the protonation of the reduced complexes. First, the electrostatic potential was determined using the linearized finite-difference Poisson-Boltzmann method,⁴⁸⁻⁵¹ as implemented in the UHBD suite of programs.⁵² The Poisson-Boltzmann calculations were performed using a 65 \times 65 \times 65 grid with a spacing of 0.25 Å, a dielectric constant of 78.5 for the solvent and 1.0 for the solute, and a probe radius of 1.4 Å. The atomic radii were taken from the parm96 parameter set for the AMBER '95 all-atom force-field.⁵³ Thus, the electrostatic potential was used to give a visual indication of the site of protonation on the reduced molecules and was displayed using GopenMol.⁵⁴ Second, the protonation energy was determined explicitly from nonlocal BLYP calculations on the optimized structures of the reduced CuGTS⁻ and CuATSM⁻ anions and their corresponding protonated forms. These quantum mechanical energies give the gas-phase protonation energy; the corresponding solution-phase protonation energy was determined from the Poisson-Boltzmann free energies of hydration.⁵⁵

Acknowledgment. We are grateful to Oxford University (G.E.D.M.), the Association for International Cancer Research (Y.Z.), and the EPSRC (R.I.M.) for support.

Supporting Information Available: Calculated geometries and energies of the copper complexes, molecular electrostatic potential for Cu(I) anions and protonated Cu(I) species, and vibrational data. This material is available free of charge via the Internet at <http://pubs.acs.org>.

References

- Blower, P. J.; Lewis, J. S.; Zweit, J. Copper radionuclides and radiopharmaceuticals in nuclear medicine. *Nucl. Med Biol.* **1996**, *23*, 957-980.
- Herrero, P.; Markham, J.; Weinheimer, C. J.; Anderson, C. J.; Welch, M. J.; Green, M. A.; Bergmann, S. R. Quantification of regional myocardial perfusion with generator-produced ⁶²Cu-PTSM and positron emission tomography. *Circulation* **1993**, *87*, 173-183.
- Mathias, C. J.; Bergmann, S. R.; Green, M. A. Development and validation of a solvent extraction technique for determination of Cu-PTSM in blood. *Nucl. Med. Biol.* **1993**, *20*, 343-349.

- (4) Fujibayashi, Y.; Taniuchi, H.; Yonekura, Y.; Ohtani, H.; Konishi, J.; Yokoyama, A. Copper-⁶²ATSM: a new hypoxia imaging agent with high membrane permeability and low redox potential. *J. Nucl. Med.* **1997**, *38*, 1155–1160.
- (5) Lewis, J. S.; McCarthy, D. W.; McCarthy, T. J.; Fujibayashi, Y.; Welch, M. J. Evaluation of ⁶⁴Cu-ATSM in vitro and in vivo in a hypoxic tumor model. *J. Nucl. Med.* **1999**, *40*, 177–183.
- (6) Lewis, J. S.; LaForest, R.; Buettner, T. L.; Song, S.-K.; Fujibayashi, Y.; Connett, J. M.; Welch, M. J. Copper-64-diacetyl-bis-(N⁴-methylthiosemicarbazone): an agent for radiotherapy. *Proc. Natl. Acad. Sci. U.S.A.* **2001**, *98*, 1206–1211.
- (7) Dearling, J. L. J.; Lewis, J. S.; Mullen, G. E. D.; Welch, M. J.; Blower, P. J. Copper bis(thiosemicarbazone) complexes as hypoxia imaging agents: structure–activity relationships. *J. Biol. Inorg. Chem.* **2002**, *7*, 249–259.
- (8) Lewis, J. S.; Sharp, T. L.; Laforest, R.; Fujibayashi, Y.; Welch, M. J. Tumor uptake of copper-diacetyl-bis(N⁴-methylthiosemicarbazone): effect of changes in tissue oxygenation. *J. Nucl. Med.* **2001**, *42*, 655–661.
- (9) Fujibayashi, Y.; Wada, K.; Taniuchi, H.; Yonekura, Y.; Konishi, J.; Yokoyama, A. Mitochondria-selective reduction of ⁶²Cu-pyruvaldehyde bis(N⁴-methylthiosemicarbazone) (⁶²Cu-PTSM) in the murine brain: a novel radiopharmaceutical for brain positron emission tomography (PET) imaging. *Biol. Pharm. Bull.* **1993**, *16*, 146–149.
- (10) Baerga, I. D.; Maickel, R. P.; Green, M. A. Subcellular distribution of tissue radiocopper following intravenous administration of ⁶⁷Cu-labeled Cu-PTSM. *Nucl. Med. Biol.* **1992**, *19*, 697–701.
- (11) Booth, B. A.; Sartorelli, A. C. Metabolic effects of copper in intact cells: comparative activity of cupric chloride and the cupric chelate of ketoxal bis(thiosemicarbazone). *Mol. Pharmacol.* **1967**, *3*, 290–302.
- (12) Petering, D. H. The reaction of 3-ethoxy-2-oxobutylaldehyde bis-(thiosemicarbazone) copper(II) with thiols. *Bioinorg. Chem.* **1972**, *1*, 273–288.
- (13) Dearling, J. L. J.; Lewis, J. S.; Mullen, G. E.; Rae, M. T.; Zweit, J.; Blower, P. J. Design of hypoxia-targeting radiopharmaceuticals: selective uptake of copper-64 complexes in hypoxic cells in vitro. *Eur. J. Nucl. Med.* **1998**, *25*, 788–792.
- (14) Dearling, J. L. J.; Lewis, J. S.; McCarthy, D. W.; Welch, M. J.; Blower, P. J. Redox active metal complexes for imaging hypoxic tissue: structure–activity relationships in copper(II) bis(thiosemicarbazone) complexes. *Chem. Commun.* **1998**, 2531–2532.
- (15) Dehdashti, F.; Mintun, M. A.; Lewis, J. S.; Govindan, R.; Welch, M. J. Evaluation of tumor hypoxia with Cu-60 ATSM and PET. *J. Nucl. Med.* **2000**, *41*, 34P.
- (16) Mintun, M. A.; Berger, K. L.; Dehdashti, F.; Lewis, J. S.; Chao, C.; Welch, M. J. Kinetic analysis of the novel hypoxic imaging agent [⁶⁰Cu]ATSM in human neoplasms. *J. Nucl. Med.* **2000**, *41*, 58P.
- (17) Takahashi, N.; Fujibayashi, Y.; Yonekura, Y.; Welch, M. J.; Waki, A.; Tsuchida, T.; Nakamura, S.; Sadato, N.; Sugimoto, K.; Yamamoto, K.; Ishii, Y. Evaluation of copper-62 ATSM in patients with lung cancer as hypoxic tissue tracer. *J. Nucl. Med.* **1998**, *39*, 53P.
- (18) Obata, A.; Fujibayashi, Y.; Miono, Y.; Waki, A.; Yonekura, Y.; Welch, M. J. Enzymes for reductive retention of Cu-Diacetyl-Bis(N⁴-Methylthiosemicarbazone) in tumour cells and their localisation in mice. *J. Labelled Compd. Radiopharm.* **2001**, *42*, S273–S275.
- (19) Minkel, D. T.; Petering, D. H. Initial reaction of 3-ethoxy-2-butyraldehyde bis(thiosemicarbazone) copper(II) with Ehrlich ascites tumour cells. *Cancer Res.* **1978**, *38*, 117–123.
- (20) Reichert, D. E.; Norrby, P. O.; Welch, M. J. Molecular modeling of bifunctional chelate peptide conjugates. 1. Copper and indium parameters for the AMBER force field. *Inorg. Chem.* **2001**, *40*, 5223–5230.
- (21) Hancock, R. In *Current Directions in Radiopharmaceutical Development*; Mather, S. J., Ed.; Kluwer Academic Publishers: The Netherlands, 1996.
- (22) Deeth, R. J.; Jenkins, H. D. B. A density functional and thermochemical study of M–X bond lengths and energies in [MX₆](2-) complexes: LDA versus Becke88/Perdew86 gradient-corrected functionals. *J. Phys. Chem. A* **1997**, *101*, 4793–4798.
- (23) Bray, M. R.; Deeth, R. J. A density functional study of active site models for xanthine oxidase. *Inorg. Chem.* **1996**, *35*, 5720–5724.
- (24) Deeth, R. J. Density-functional study of the tetraoxometalates of CrVI, MnVI And FeVI. *J. Chem. Soc. Faraday Trans.* **1993**, *89*, 3745–3749.
- (25) Deeth, R. J. Is the Ground-State of [RuO₄](2-) Exceptional? *J. Chem. Soc. Dalton Trans.* **1995**, 1537–1542.
- (26) Bray, M. R.; Deeth, R. J.; Paget, V. J.; Sheen, P. D. The relative performance of the local density approximation and gradient-corrected density functional theory for computing metal–ligand distances in Werner-Type and organometallic complexes. *Int. J. Quantum Chem.* **1997**, *61*, 85–91.
- (27) Deeth, R. J. Soft cobalt(III) centres: electronic leveling in [CoX₃(AH(3))(2)] (X = Cl, Br or I; A = P, As or Sb). *J. Chem. Soc. Dalton Trans.* **1997**, 4203–4207.
- (28) Deeth, R. J. Theoretical Molecular-Structures and Vibrational Frequencies for the Dioxodihalides of Chromium(VI) and Molybdenum(VI). *J. Phys. Chem.* **1993**, *97*, 11625–11627.
- (29) Jones, C. J.; McCleverty, J. A. Complexes of transition metals with Schiff bases and the factors influencing their redox properties. Part I. Nickel and copper complexes of some diketone bis-thiosemicarbazones. *J. Chem. Soc. A* **1970**, 2829–2836.
- (30) Wolfe, J. J.; Wright, J. D.; Reynolds, C. A.; Saunders, A. C. Electrode potentials for bioreductive agents from neural networks. *Anticancer Drug Des.* **1994**, *9*, 85–102.
- (31) Wu, J. H.; Reynolds, C. A. Energetics of reactions involving transition metal complexes: calculation of relative electrode potentials for cobalt complexes at various ionic strengths using density functional and Poisson–Boltzmann methods. *J. Am. Chem. Soc.* **1996**, *118*, 10545–10550.
- (32) Reynolds, C. A.; King, P. M.; Richards, W. G. Computed redox potentials and the design of bioreductive agents. *Nature* **1988**, *334*, 80–82.
- (33) Anglada, M. C.; Farrera, J.-A.; Ribó, J. M. One-electron Redox Processes of the Cu(II) chelate of 3,8,12,17-tetraethyl-2,7,13,18-tetramethylbilin-1,19-dione. *Tetrahedron Lett.* **1997**, *38*, 669–672.
- (34) Scheidt, W. R.; Reed, C. A. Spin-state stereochemical relationships in iron porphyrins – implications for the hemoproteins. *Chem. Rev.* **1981**, *81*, 543–555.
- (35) Casas, J. S.; Castineiras, A.; Rodriguez-Arguelles, M. C.; Sanchez, A.; Sordo, J.; Vazquez-Lopez, A.; Vazquez-Lopez, E. M. Reactions of diorganotin(IV) oxides with isatin 3-and 2-thiosemicarbazones and with isatin 2,3-bis(thiosemicarbazone): influence of diphenyldithiophosphinic acid (isatin=1H-indole-2,3-dione). *J. Chem. Soc. Dalton Trans.* **2000**, 4056–4063.
- (36) Gingras, B. A.; Suprunchuk, R. W.; Bayley, C. H. The preparation of some thiosemicarbazones and their copper complexes. *Can. J. Chem.* **1962**, *40*, 1053–1059.
- (37) Parr, R. G.; Yang, W. *Density Functional Theory of Atoms and Molecules*; OUP: New York, 1989.
- (38) Andezelm, J.; Wimmer, E. Density functional Gaussian-type-orbital approach to molecular geometries, vibrations and reaction energies. *J. Chem. Phys.* **1992**, *96*, 1280–1303.
- (39) Unichem 4.1 and 5.1, Oxford Molecular, Medawar Centre, Oxford, U.K. 2000, Ref Type: Computer Program.
- (40) Becke, A. D. Density-functional exchange-energy approximation with correct asymptotic behaviour. *Phys. Rev. A* **2001**, *38*, 3098–3100.
- (41) Lee, C.; Yang, W.; Parr, R. G. Development of the Colle-Salvetti correlation-energy formula into a functional of the electron-density. *Phys. Rev. B* **1988**, *37*, 785–789.
- (42) Perdew, J. P.; Wang, Y.; Ziesche, P. E. H., Ed. Akademie Verlag: Berlin, 1991.
- (43) Hamprecht, F. A.; Cohen, A. J.; Tozer, D. J.; Handy, N. C. Development and assessment of new exchange-correlation functionals. *J. Chem. Phys.* **1998**, *109*, 6264–6271.
- (44) Vosko, S. H.; Wilk, L.; Nusair, M. Accurate spin-dependent electron liquid correlation energies for local spin density calculations: a critical analysis. *Can. J. Phys.* **1980**, *58*, 1200–1211.
- (45) Godbout, N.; Salahub, D. R.; Andezelm, J.; Wimmer, E. Optimisation of Gaussian-type basis-sets for local spin-density functional calculations. 1. Boron Through Neon, optimisation technique and validation. *Can. J. Chem.* **1992**, *70*, 560–571.
- (46) Pople, J. A.; Nesbet, R. K. Self-consistent orbitals for radicals. *J. Chem. Phys.* **1954**, *22*, 571–578.
- (47) John, E.; Fanwick, P. E.; McKenzie, A. T.; Stowell, J. G.; Green, M. A. Structural characterization of a metal-based perfusion tracer: copper(II) pyruvaldehyde bis(N⁴-methylthiosemicarbazone). *Int. J. Radiat. Appl. Instrum. B* **1989**, *16*, 791–797.
- (48) Luty, B. A.; Davis, M. E.; Mcammon, J. A. Solving the finite-difference nonlinear poisson-boltzmann equation. *J. Comput. Chem.* **1992**, *13*, 1114–1118.
- (49) Warwicker, J.; Watson, H. Calculation of the electric-potential in the active-site cleft due to alpha-helix dipoles. *J. Mol. Biol.* **2001**, *157*, 671–679.
- (50) Sharp, K. A.; Honig, B. Electrostatic interactions in macromolecules – theory and applications. *Annu. Rev. Biophys. Biophys. Chem.* **1990**, *19*, 301–332.
- (51) Honig, B.; Sharp, K.; Yang, A. S. Macroscopic models of aqueous-solutions – biological and chemical applications. *J. Phys. Chem.* **1993**, *97*, 1101–1109.
- (52) Davis, M. E.; Madura, J. D.; Sines, J.; Luty, B. A.; Allison, S. A.; Mcammon, J. A. Diffusion-controlled enzymatic reactions. *Methods Enzymol.* **1991**, *202*, 473–497.

- (53) Cornell, W. D.; Cieplak, P.; Bayly, C. I.; Gould, I. R.; Merz, K. M.; Ferguson, D. M.; Spellmeyer, D. C.; Fox, T.; Caldwell, J. W.; Kollman, P. A. A 2nd generation force-field for the simulation of proteins, nucleic-acids, and organic molecules. *J. Am. Chem. Soc.* **1995**, *117*, 5179–5197.
- (54) Laaksonen, L. A graphics program for the analysis and display of molecular dynamics trajectories. *J. Mol. Graph.* **1992**, *10*, 33–4, 24.
- (55) Jean-Charles, A.; Nicholls, A.; Sharp, K.; Honig, B.; Tempczyk, A.; Hendrickson, T. F.; Still, W. C. Electrostatic contributions to solvation energies – comparison of free-energy perturbation and continuum calculations. *J. Am. Chem. Soc.* **1991**, *113*, 1454–1455.

JM0104217